Monthly Notices
of the
ROYAL ASTRONOMICAL SOCIETY

MNRAS **494,** 4606–4615 (2020)
Advance Access publication 2020 April 18

doi:10.1093/mnras/staa1028

Propanal, an interstellar aldehyde – first infrared band strengths and other properties of the amorphous and crystalline forms

Yuki Y. Yarnall,[1,2] Perry A. Gerakines[2] and Reggie L. Hudson[2]★

[1] *Universities Space Research Association, Greenbelt, MD 20771, USA*
[2] *Astrochemistry Laboratory, NASA Goddard Space Flight Center, Greenbelt, MD 20771, USA*

Accepted 2020 April 8. Received 2020 January 23; in original form 2020 January 23

ABSTRACT

Chemical evolution in molecular clouds in the interstellar medium is well established, with the identification of over 200 molecules and molecular ions. Among the classes of interstellar organic compounds found are the aldehydes. However, laboratory work on the aldehydes has scarcely kept pace with astronomical discoveries as little quantitative solid-phase infrared (IR) data have been published on any of the aldehydes, and the same is true for important properties such as density, refractive indices, and vapour pressures. In this paper, we examine the IR spectra of solid propanal ($HC(O)CH_2CH_3$, propionaldehyde), along with several physical properties, for both the amorphous and crystalline forms of the compound. The quantitative measurements we report, such as IR intensities and optical constants, will be useful in laboratory investigations of the formation and evolution of propanal-containing ices, will serve as benchmark data for theoretical investigations, and will inform observational studies.

Key words: astrochemistry – methods: laboratory – astrochemistry – ISM: molecules.

1 INTRODUCTION

Propanal, $HC(O)CH_2CH_3$, is one of six aldehydes that have been identified in molecular clouds, the other five being formaldehyde (H_2CO), acetaldehyde ($HC(O)CH_3$), propynal ($HC(O)C_2H$), glycolaldehyde ($HC(O)CH_2OH$), and propenal ($HC(O)CHCH_2$) (see Fig. 1 and the review paper of McGuire 2018). The first detection of propanal, also called propionaldehyde, was by the observation of rotational transitions towards the star formation region Sagittarius B2(N) (Hollis et al. 2004). Propanal also was detected towards the low-mass protostar IRAS 16293–2422 using the Atacama Large Millimeter/submillimeter Array (Lykke et al. 2017). Propanal was reported in the Murchison meteorite Jungclaus et al. (1976), and appears to have been found in comet 67P Churyumov/Gerasimenko by time-of-flight mass spectrometry, along with acetone, a propanal isomer (Goesmann et al. 2015; Altwegg et al. 2017; Schuhmann et al. 2019).

Propanal has been reported several times as a reaction product in low-temperature laboratory studies designed to probe the chemistry of icy extraterrestrial environments. Examples of such work include $CO + CH_4$ and $C^{18}O + C_2H_6$ ices warmed after electron irradiation at ∼5 K (Kaiser, Maity & Jones 2014; Abplanalp et al. 2016) and an ultraviolet-photolysed $H_2O + {}^{13}CH_3OH + NH_3$ ice warmed to room temperature (de Marcellus et al. 2015). Hudson, Loeffler & Yocum (2017a) reported an *in situ* detection of propanal in $CO_2 + C_3H_6$ ices that were proton irradiated at 10 K, the detection being with infrared (IR) spectroscopy, also at 10 K.

In addition to investigations of ice photo- and radiation chemistry, several laboratory studies have examined reactions of hydrogen atoms in ices, and some such studies have involved propanal. Both Jonusas, Guillemin & Krim (2017) and Krim et al. (2018) investigated the possible hydrogenation of propanal near 10 K, but no reduction products (i.e. alcohols) were detected using mid-IR spectroscopy, leading the authors to comment on solid propanal's stability against H-atom bombardment at low temperatures. In contrast, Qasim et al. (2019) observed 1-propanol ($CH_3CH_2CH_2OH$) by mass spectrometry on warming a propanal ice that had been exposed to H atoms at 10 K.

Laboratory studies are essential for the accurate interpretation of IR spectra of ices from both terrestrial and astronomical observations. In the case of propanal, several research groups have published spectra of solid forms of the compound. Sbrana and Schettino (1970) published mid-IR transmission spectra of crystalline propanal at 83 K along with peak assignments, the ice being made by vapour-phase deposition onto a CsI substrate. Similar IR spectra of crystalline propanal were published by Frankiss and Kynaston (1972) and Guirgis et al. (1998). Crystalline propanal ices over a range of thicknesses were examined at 120 K by Dostert et al. (2016). Mid-IR spectra of amorphous propanal at ∼10 K also have been reported by several groups, in each case the ice being held on a metal surface and the spectra being obtained in a reflection-absorption mode (Jonusas et al. 2017; Krim et al. 2018; Qasim et al. 2019).

★ E-mail: reggie.hudson@nasa.gov

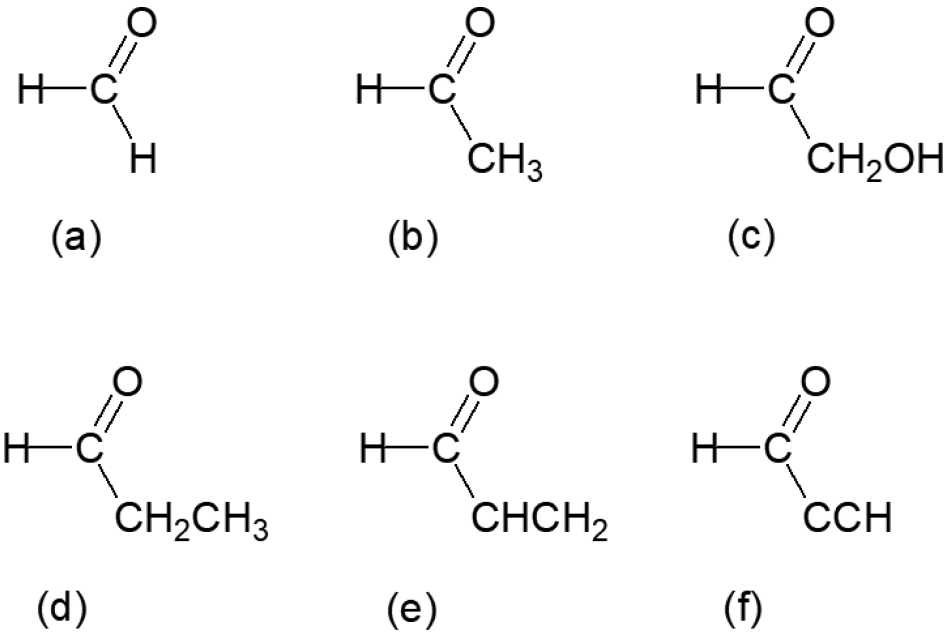

Figure 1. Structures of aldehydes identified in the interstellar medium. (a) formaldehyde, (b) acetaldehyde, (c) glycolaldehyde, (d) propanal (propionaldehyde), (e) propenal (acrolein), and (f) propynal.

However, aside from peak positions and bandwidths, little quantitative IR spectral information is available for solid propanal to assist in studies of this interstellar compound. More specifically, quantitative measures of IR intensities, such as band strengths and absorption coefficients for peaks, are lacking, hindering quantitative studies of propanal in interstellar ices and their laboratory analogues. This work was undertaken to address this gap in the literature.

In this paper, we report the first measurements of mid-IR band strengths and absorption coefficients for propanal ices, along with the first measurements of refractive indices and ice densities for propanol ices, quantities on which determinations of IR intensities are based. We also present optical constants for each solid form of propanal, along with vapour pressures and a sublimation enthalpy for the crystalline phase. Note that this work is an extension of our recent study of the next smaller aldehyde, acetaldehyde, and so the goals and methods in this paper resemble those in that work (Hudson & Ferrante 2020).

2 EXPERIMENTAL SECTION

Reagent-grade propanal was purchased from Sigma Aldrich, degassed by multiple freeze-pump-thaw cycles with liquid nitrogen before use, and stored at 3°C between experiments. The procedures and equipment for measuring refractive indices (n, 670 nm) and densities (ρ in g cm^{-3}) of ices are as described in several of our recent papers, which should be consulted for details (Hudson, Ferrante & Moore 2014; Hudson, Loeffler & Gerakines 2017b). Briefly, two-laser interferometry gave n_{670} from interference fringes, measured during the ice's growth, and a quartz crystal microbalance (QCM, Inficon IC6) gave ice densities (Tempelmeyer & Mills 1968; Lu & Lewis 1972). The ultrahigh vacuum (UHV) chamber in which such measurements were made had a base pressure of $\sim 10^{-10}$ Torr at 19 K. IR spectra (Thermo Nicolet Nexus 6700 spectrometer, MCT detector) were recorded of each propanal ice to verify its form (amorphous or crystalline). After an ice was prepared and its spectrum recorded, the sample was warmed at about 1 K min^{-1} until it sublimed. Measurements of the frequency of the QCM during such warmings provided sufficient data from which vapour pressures could be calculated, along with an enthalpy of sublimation (see Section 3.3 for details of the data analysis method).

Mid-IR transmission spectra of amorphous and crystalline propanal of various thickness were recorded as 100-scan accumulations with a Thermo iS 50 spectrometer (DTGS detector) at a resolution of 1 cm^{-1} from 4000 to 600 cm^{-1}, all ices being made by vapour-phase deposition onto a precooled CsI substrate. Interference fringes recorded during ice formation were measured with a laser (670 nm) as in our earlier work (e.g. Hudson et al. 2017b), and used to calculate each ice's thickness (h) according to equation (1)

$$h = \frac{\mathrm{N_{fringes}}\lambda}{2\sqrt{n_{670}^2 - \sin^2\theta}}, \quad (1)$$

where N_{fringes} is the number of interference fringes recorded during a deposition, $\theta \approx 0^\circ$, the angle between the laser's beam and a line drawn perpendicular to the CsI substrate, and n_{670} is the refractive index found by two-laser interferometry (see Heavens 2011 for more on this method of thickness determination).

Propanal ice samples prepared at ~10 K were amorphous solids, samples prepared at 100 K were crystalline. For each type of ice, mid-IR transmission spectra were recorded for samples of various thicknesses in order to determine propanal band strengths (A') and absorption coefficients (α'), as explained later and, again, as described in our previous papers (e.g. Hudson et al. 2014). Errors and uncertainties for A' and α' are discussed in Hudson et al. (2017b) and are of the order of 5 per cent, and less for the stronger IR features.

3 RESULTS

3.1 Refractive indices and densities

Three amorphous and five crystalline propanal ices were prepared for measurements of refractive indices and densities. The average refractive index and density at 19 K for the amorphous ices were $n_{670} = 1.326$ and $\rho = 0.778$ g cm^{-3}. Similarly, the average refractive index and density at 100 K for crystalline propanal were $n_{670} = 1.524$ and $\rho = 1.105$ g cm^{-3}. Uncertainties (i.e. standard errors) for n_{670} and ρ were of the order of $\pm$ 0.005 and $\pm$ 0.005 g cm^{-3}, respectively. These values of n_{670} and ρ were used to determine absorption coefficients and band strengths of our propanal ices.

3.2 Mid-IR spectra

Fig. 2 shows mid-IR survey spectra of solid $HC(O)CH_2CH_3$ ices made by vapour-phase deposition at 10 (amorphous ice) and 100 K (crystalline ice), with a thickness of about 1 μm in each case. Figs 3–5 show expansions of several regions. Spectra in each figure are offset for clarity. Warming amorphous propanal from a deposition temperature of 10 K resulted in the ice's irreversible crystallization near 93 K, the spectra resembling those shown at 100 K in our figures.

Our propanal spectra of Figs 2–5 resemble those previously published, allowing for the fact that earlier spectra of the amorphous solid were recorded in a reflection mode, which can alter relative intensities. To quantify IR intensities, both absorption coefficients and band strengths, we recorded IR spectra of five amorphous ices, with thicknesses of about 0.25 to 1.1 μm, and six crystalline ices, with thicknesses of about 0.25 to 2 μm. Peak heights and band areas were measured to determine apparent absorption coefficients α' and apparent band strengths A'. For example, Fig. 6 shows three typical Beer's Law plots from which A' values were found, all correlation coefficients being greater than 0.99. Tables 1 and 2 list peak positions, regions for integrations, and IR intensities for amorphous, and crystalline propanal. Spectral assignments are taken from earlier papers. Note that most regions integrated include more than one absorbance feature.

Another way to quantify IR spectra and spectral intensities is with the complex index of refraction $n - ik$, the real (n) and imaginary (k) components being referred to as optical constants. We calculated n and k for amorphous and crystalline propanal by an iterative Kramers–Kronig method (e.g. Hudgins et al. 1993; Moore et al. 2010) using our measured n_{670} and our IR spectra. Figs 7 and 8 show the optical constants of amorphous and crystalline propanal, respectively, and an electronic version of these constants is on our webpages (https://science.gsfc.nasa.gov/691/cosmicice/constants.html). Optical constants allow for the calculation of spectra obtained in a transmission mode, as well as by reflection at various angles from a metal substrate.

Besides the IR peaks listed in our tables, numerous other features can be seen in our spectra. Weaker absorbances include various ^{13}C isotopic peaks, combination bands, and overtones, such as the peak near 3405 cm^{-1} for the first overtone of ν(C=O stretch, ~1730 cm^{-1}). We did not study or tabulate any of these weaker features, but they can be found in earlier papers (Sbrana & Schettino 1970; Frankiss & Kynaston 1972). Of particular interest is a very large peak near 1695 cm^{-1}, an overtone of the ~855 cm^{-1} vibration, but with a shift and a greatly enhanced intensity due to Fermi resonance with the ν(C=O) stretching fundamental (Sbrana & Schettino 1970). In fact, propanal's two large peaks in the 1700 cm^{-1} region were useful in our recent study of the radiolytic oxidation of 1-propanol at interstellar temperatures (Hudson and Moore 2018).

3.3 Vapour pressures and enthalpy of sublimation

Warming an ice sample in our UHV chamber initiated propanal sublimation, which was monitored by recording the corresponding frequency changes of our QCM in real time. The rise in the balance's oscillation frequency was used to calculate mass-loss from the metal substrate, corresponding to the flux (F) of propanal molecules moving from the ice phase to the vapour phase, following a method similar to that of Luna et al. (2012).

In summary, the frequency of the microbalance (f in Hz) was measured at regular time intervals while increasing the temperature of the ice sample at a constant rate (~1 K min^{-1}). Prior knowledge of the temperature dependence of the microbalance frequency without a sample present (f_0 in Hz) then allowed us to determine the sample's mass per unit area on the microbalance (μ in g cm^{-2}) from

$$\mu = \kappa \left(\frac{1}{f} - \frac{1}{f_0} \right), \tag{2}$$

where $\kappa = 4.42 \times 10^5$ Hz g cm^{-2} is a constant that encapsulates the physical properties of the type of quartz crystal used in the microbalance (Lu & Lewis 1972). The flux F (in molecules cm^{-2} s^{-1}) was then obtained from the rate of change of μ, which, in turn, gave vapour pressures from

$$P = F \sqrt{2\pi m k T}, \tag{3}$$

where m is the mass of a propanal molecule. The usual Clausius–Clapeyron plot then gave an enthalpy of sublimation ($\Delta H_{\rm subl}$) for propanal.

Fig. 9 shows the results of one propanal warming experiment. Fig. 9(a) shows the quartz crystal's oscillation frequency (f) as the temperature of the microbalance was increased at 1 K min^{-1}. The same panel also contains the QCM frequencies without a sample present on the microbalance (f_0) over the same temperature range. Propanal sublimation was first detected near 120 K, and the two sets of data converge near 145 K, where the sample is completely sublimated in this experiment. Figs 9(b) and 9(c) contain the corresponding graphs for the mass per unit area of the sample (μ) and the flux of subliming molecules (F), respectively. Fig. 9(d) shows the logarithm of the derived vapour pressure (P) vs. 1/T. A least-squares fit to the linear portion of the data in Fig. 9(d) was used to derive $\Delta H_{\rm subl}$ for this experiment in the usual way (i.e. $\Delta H_{\rm subl} = -R \times$ slope), and a value of 46.09 $\pm$ 0.03 kJ mole^{-1} was obtained from an average of three separate measurements. A list of derived vapour pressures is given in Table 3, where the uncertainties listed are from the propagation of the uncertainties in each linear fit. As a check, we performed similar warm-up experiments and derived vapour pressures for both H_2O and CO_2. Within the uncertainties in our data, our results agreed with the literature (Khanna et al. 1990, Murphy & Koop 2005, and references therein).

3.4 Propanal purity

One concern we had when beginning this work was our propanal's purity, since the compound forms azeotropic mixtures with H_2O (Smith & Bonner 1951). We first compared IR spectra of propanal ices prepared from the reagent received from our supplier to the

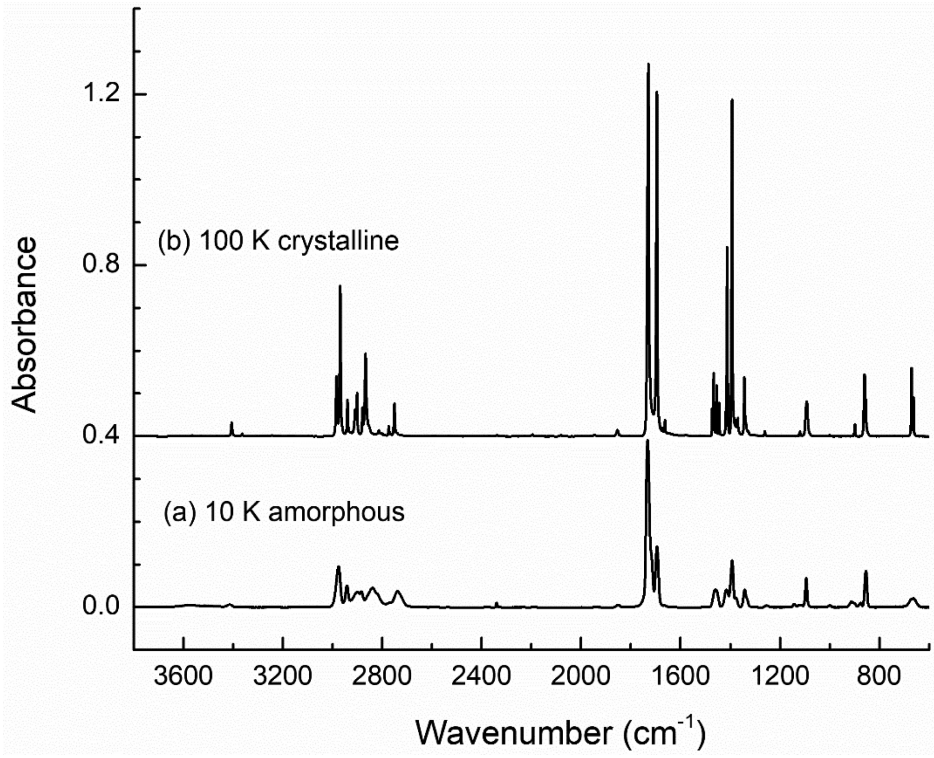

Figure 2. Mid-IR survey spectra of (a) amorphous and (b) crystalline propanal prepared by vapour-phase deposition onto a CsI substrate at 10 and 100 K, respectively. The original thickness of each ice was about 1 μm.

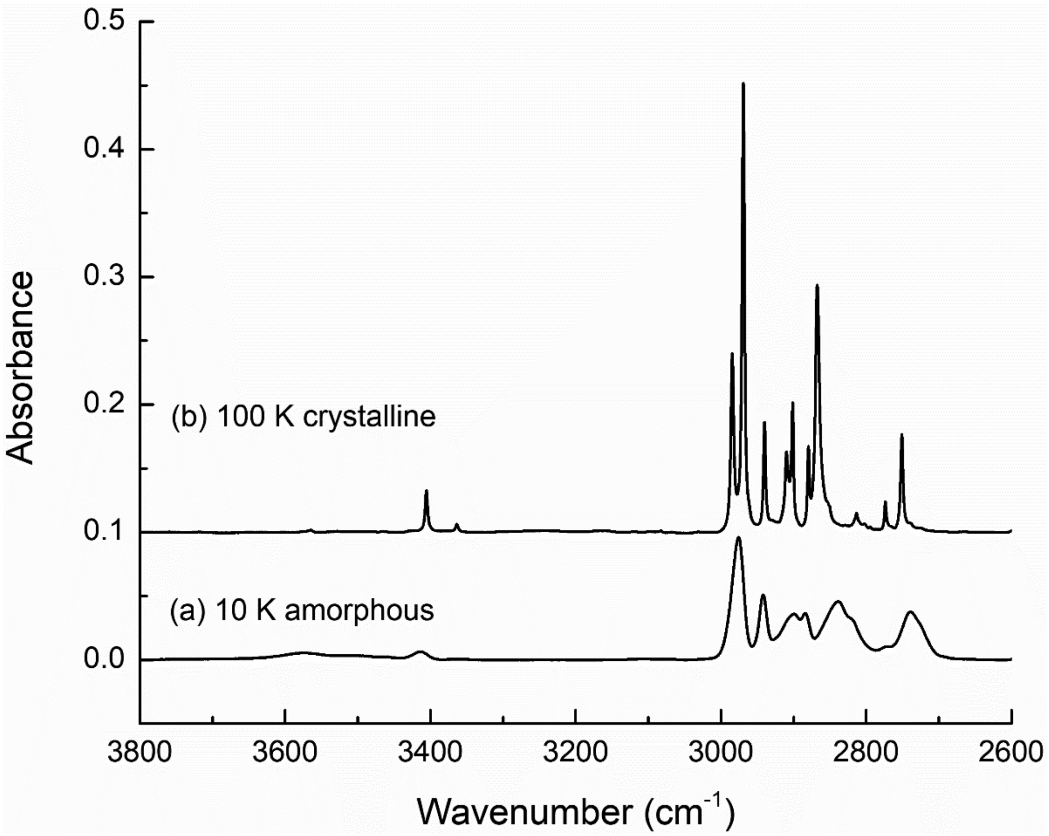

Figure 3. Spectra of amorphous and crystalline propanal between 3800 and 2600 cm^{-1}.

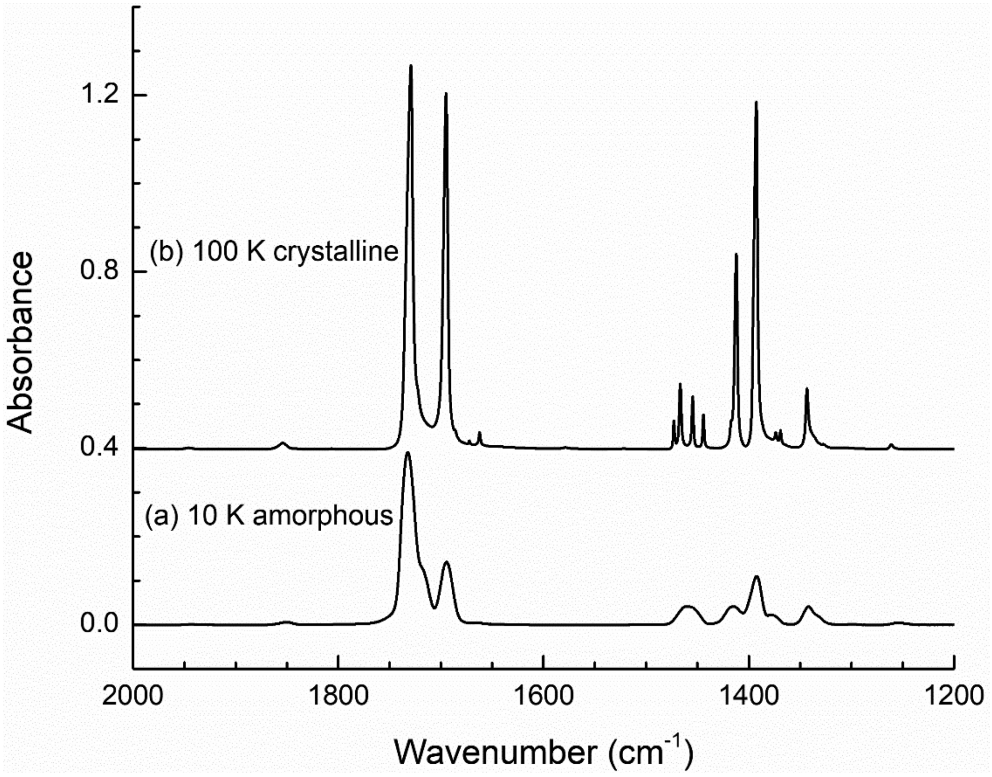

Figure 4. Spectra of amorphous and crystalline propanal between 2000 and 1200 cm^{-1}.

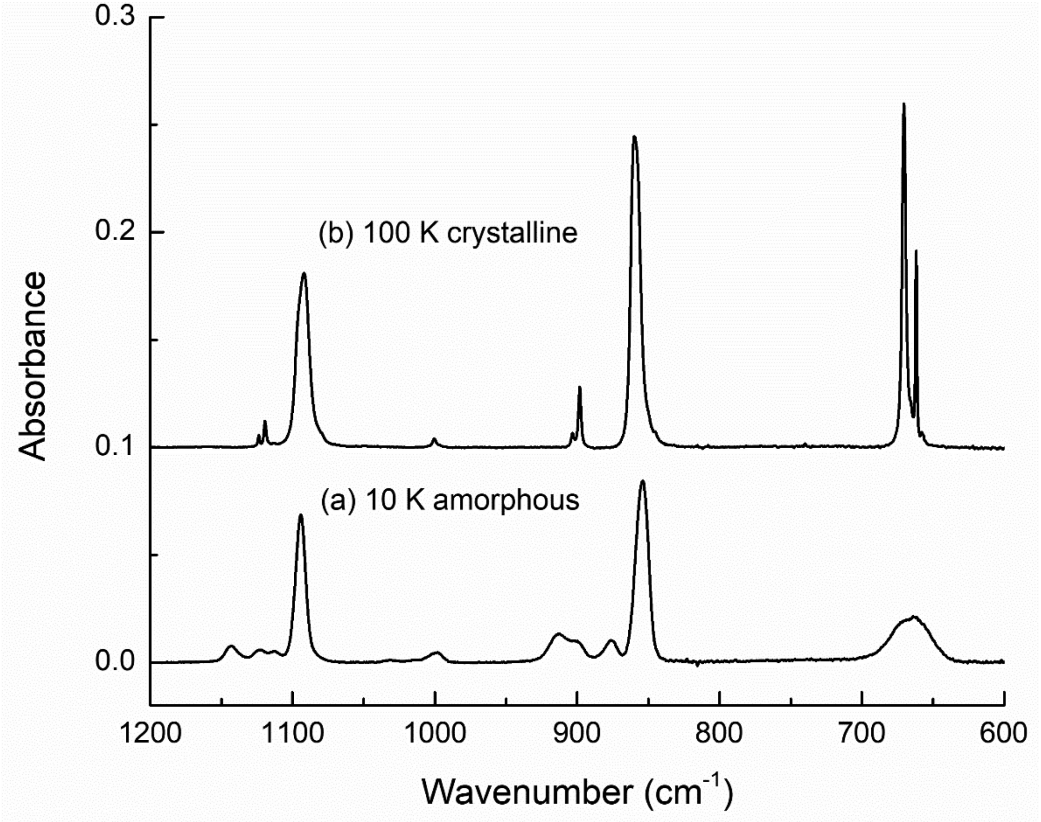

Figure 5. Spectra of amorphous and crystalline propanal between 1200 and 600 cm^{-1}.

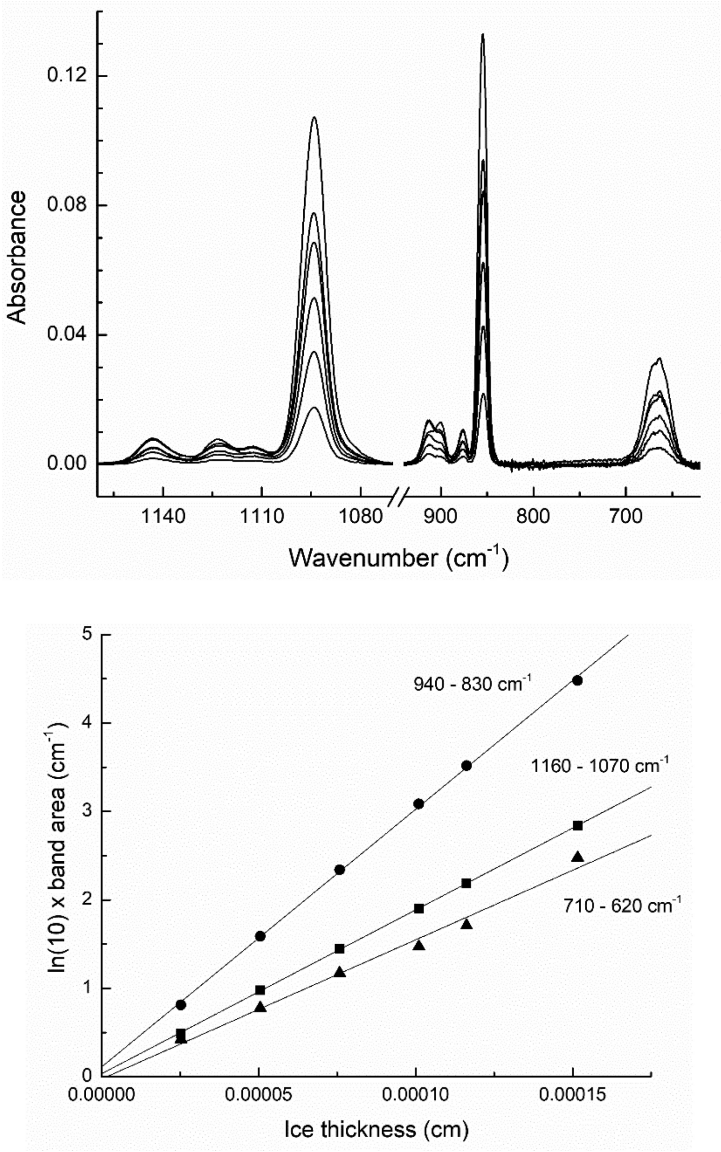

Figure 6. Representative Beer's Law plots for the determination of apparent band strengths (*A*') of amorphous propanal for three IR features. Spectra are in the upper panel and the corresponding Beer's Law curves are in the lower panel. Note that the upper panel has two different horizontal scales before and after the axis break.

IR spectra of ices prepared from the same liquid, but after drying with anhydrous magnesium sulfate ($MgSO_4$), a common laboratory desiccant. Few, if any, differences were found between the IR spectra of the two ices. In one experiment, we warmed an ice to ∼145 K to drive off propanal, leaving a very small residual absorbance near 3300 cm^{-1}, which might have been from H_2O ice. Using the optical-constants data of Hudgins et al. (1993), we estimated that the initial H_2O contamination was no more than 0.3 per cent, which would have a negligible influence on our results.

Our Fig. 9(a) shows a more severe test for H_2O contamination. Near 140 K and higher, the data (i.e. frequencies) from the run in which the QCM was warmed with no propanal sample present, a control or blank run, matches the data for the run in which propanal was deposited on the microbalance at a lower temperature and then warmed. The convergence of the two sets of data near 140 K suggests that any H_2O initially present in the ice and then left behind after propanal sublimation was indeed small, in agreement with our IR measurements (see Luna et al. 2012 for a similar argument for QCM measurements with solid CO_2).

4 DISCUSSION

4.1 Densities and refractive indices

We have not found previous measurements of either densities or refractive indices of solid propanal for comparison to those reported here. In our experience (Hudson et al. 2020), the density and refractive index values of the amorphous form of an ice are slightly smaller than those of the crystalline form, a trend that is followed for propanal. The values of n_{670} and ρ for our amorphous propanal differ from those of liquid propanal at 20°C (n_D = 1.362, ρ = 0.797 g cm^{-3}, Smith & Bonner 1951) by only about 3 per cent. Values of n_{670} and ρ for our crystalline ices show greater deviations

Table 1. Intensities of selected IR absorptions of amorphous propanal at 10 K.[a]

Peak position (cm^{-1})	α' (cm^{-1})	Integration range (cm^{-1})	A' (10^{-18} cm molecule^{-1})	Approximate description[b]
2976	1980	3050–2650	19.1	CH_3 asym str
1732	9020	1800–1600	23.2	C=O str
1460	867	1490–1440	2.01	CH_3 asym def
1392	2620	1440–1360	5.86	CH_3 sym def
1342	955	1360–1310	1.58	CH_2 wagging
1094	160	1160–1070	1.98	CH_3 rocking
854	1980	940–830	3.11	CCC sym str
666	491	710–620	1.95	CH_2 rock + OCC bend

[a]For each peak and integration range, α' is the slope of a Beer's Law graph of ln(10) × (peak height) against ice thickness, and A' is the slope of ln(10) × (band area) against ice thickness divided by ($\rho N_A/M$), where $\rho = 0.778$ g cm^{-3}, $N_A = 6.022 \times 10^{23}$ molecule mol^{-1}, and M is the molar mass of propanal (58.8 g mol^{-1}). Ice thicknesses were calculated with equation (1) using $n_{670} = 1.326$. A' is rounded to three significant figures in all cases.
[b]Assignments from Guirgis et al. (1998) with asym = asymmetric, sym = symmetric, def = deformation, and str = stretching.

Table 2. Intensities of selected IR absorptions of crystalline propanal at 100 K[a]

Peak position (cm^{-1})	α' (cm^{-1})	Integration range (cm^{-1})	A' (10^{-18} cm molecule^{-1})	Approximate description[b]
2969	8860	3050–2650	14.5	CH_3 asym str
1729	20 800	1780–1590	23.6	C = O str
1467	3590	1490–1430	1.98	CH_3 asym def
1393	1820	1430–1354	10.4	CH_3 sym def
1343	3340	1354–1280	1.42	CH_2 wagging
1092	1900	1110–1070	1.59	CH_3 rocking
860	3830	880–820	2.99	CCC sym str
670	4060	690–640	1.84	CH_2 rock + OCC bend

[a]Determinations of α' and A' are the same as in Table 1 except that $\rho = 1.105$ g cm^{-3} and $n_{670} = 1.524$ were used for crystalline propanal. A' is rounded to three significant figures in all cases.
[b]Assignments from Guirgis et al. (1998) with asym = asymmetric, sym = symmetric, def = deformation, and str = stretching.

for both n (11 per cent) and ρ (27 per cent) from the liquid, as expected. Our data gave a molar refraction (R_M) for amorphous propanal that is only about 6 per cent smaller than that of the crystalline ice.

4.2 IR spectra

The overall agreement between our IR spectra in Figs 2–5, and our peak positions of Tables 1 and 2, and similar results from earlier workers is quite good, even allowing for differences in the ways that the ice samples were prepared or the methods for recording IR spectra. The mid-IR spectra presented here for amorphous propanal appear to be the first such conventional transmission spectra available, previous results being from reflection-transmission measurements of solid propanal on a metal surface. This difference is important as band intensities and peak absorption coefficients can vary between transmission and reflection measurements (see e.g. Abdulgalil et al. 2013). Our amorphous-ice spectrum in Fig. 2 closely resembles the liquid-phase transmission spectrum of Guirgis et al. (1998), which is reasonable considering that an amorphous ice can be considered a frozen version of a liquid. That same paper reports peak positions for two conformations of propanal, with the *cis* isomer being the more abundant and more stable. All of the positions in our Tables 1 and 2 agree with the *cis* identification.

The main new information in this paper concerns our direct measurements of IR intensities. Our values of α' and A' in Tables 1 and 2 depend on ice density and refractive index, which we have measured directly for both forms of solid propanal for the first time. This leads to greater confidence in our intensity results than would otherwise be possible. We have not found any comparable direct measurements of solid propanal's IR intensities in the literature. However, Jonusas et al. (2017) report indirect measurements for two IR regions, near 3000 and 1700 cm^{-1}, with the resulting A' values being about 50 per cent of our own, a variation that probably is influenced by different choices of integration limits.

Our IR optical constants also are, to our knowledge, the first of their type. From this one can calculate absolute absorption coefficients (α) from

$$\alpha\ (\tilde{\nu}) = 4\pi\tilde{\nu}k\,(\tilde{\nu}) \tag{4}$$

and absolute band strengths (A) from

$$A = \frac{1}{\rho_N}\int_{\tilde{\nu}_1}^{\tilde{\nu}_2} \alpha\,(\tilde{\nu})\,\mathrm{d}\tilde{\nu} \tag{5}$$

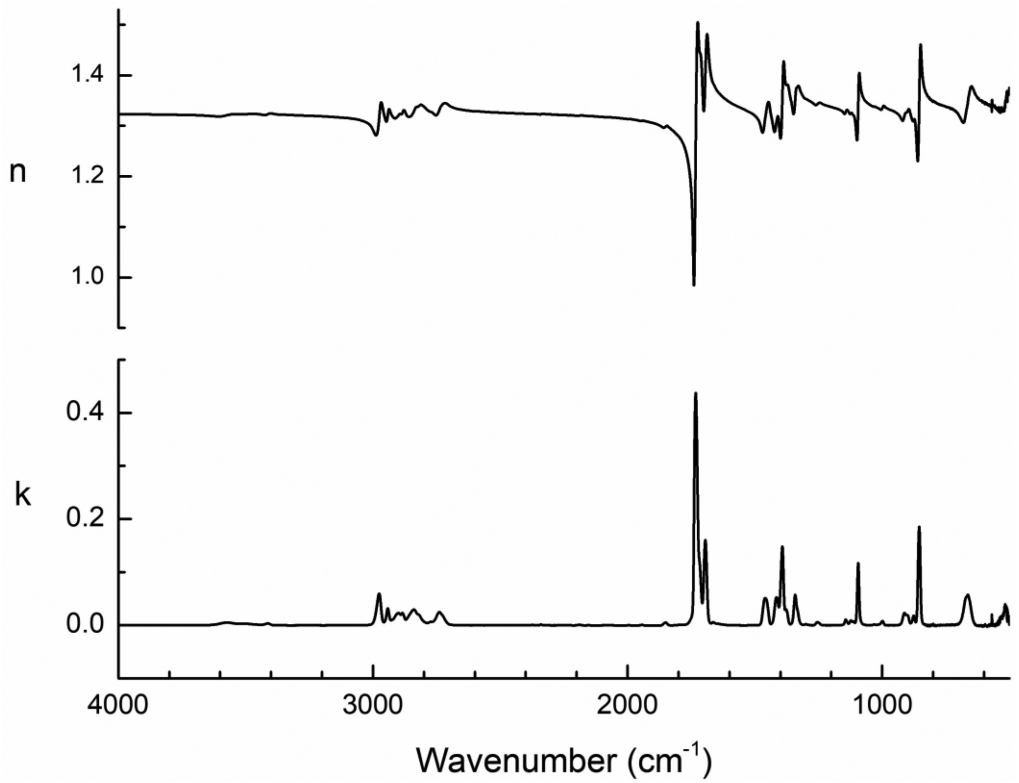

Figure 7. Optical constants for amorphous propanal at 10 K.

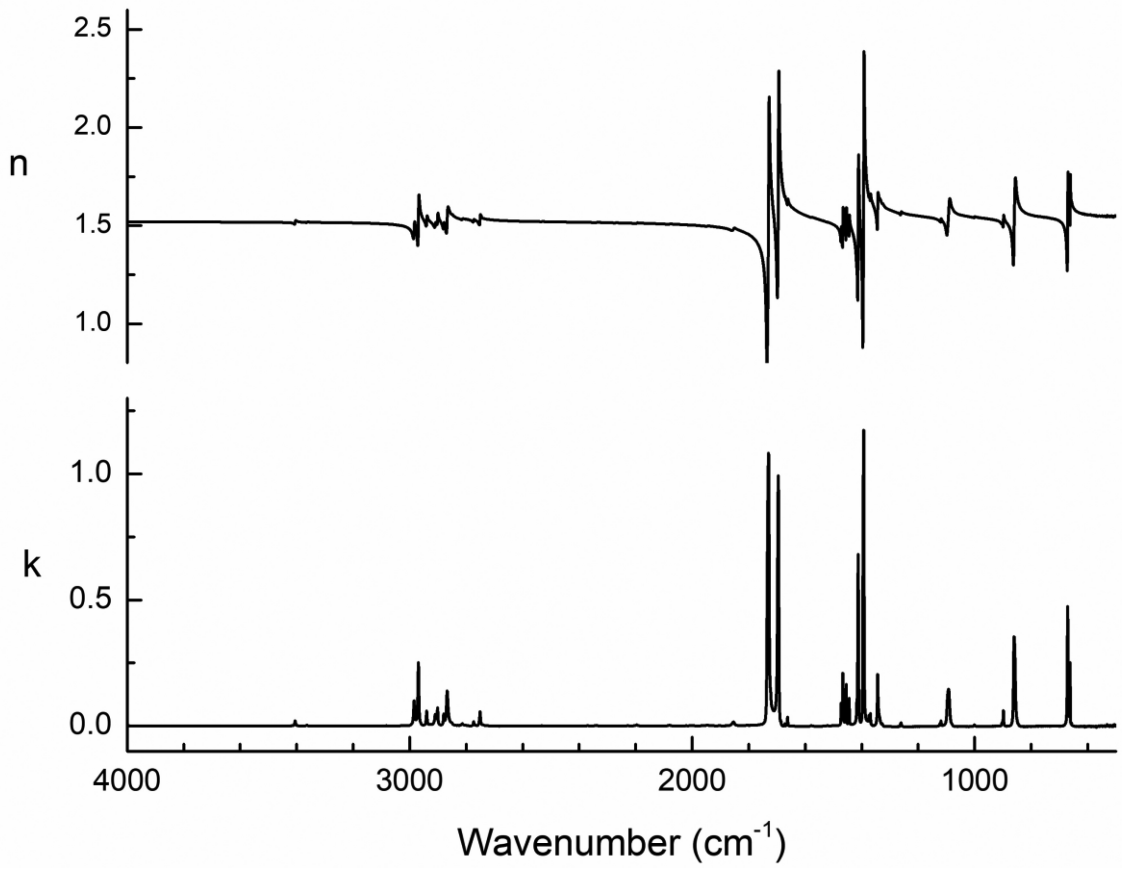

Figure 8. Optical constants for crystalline propanal at 100 K.

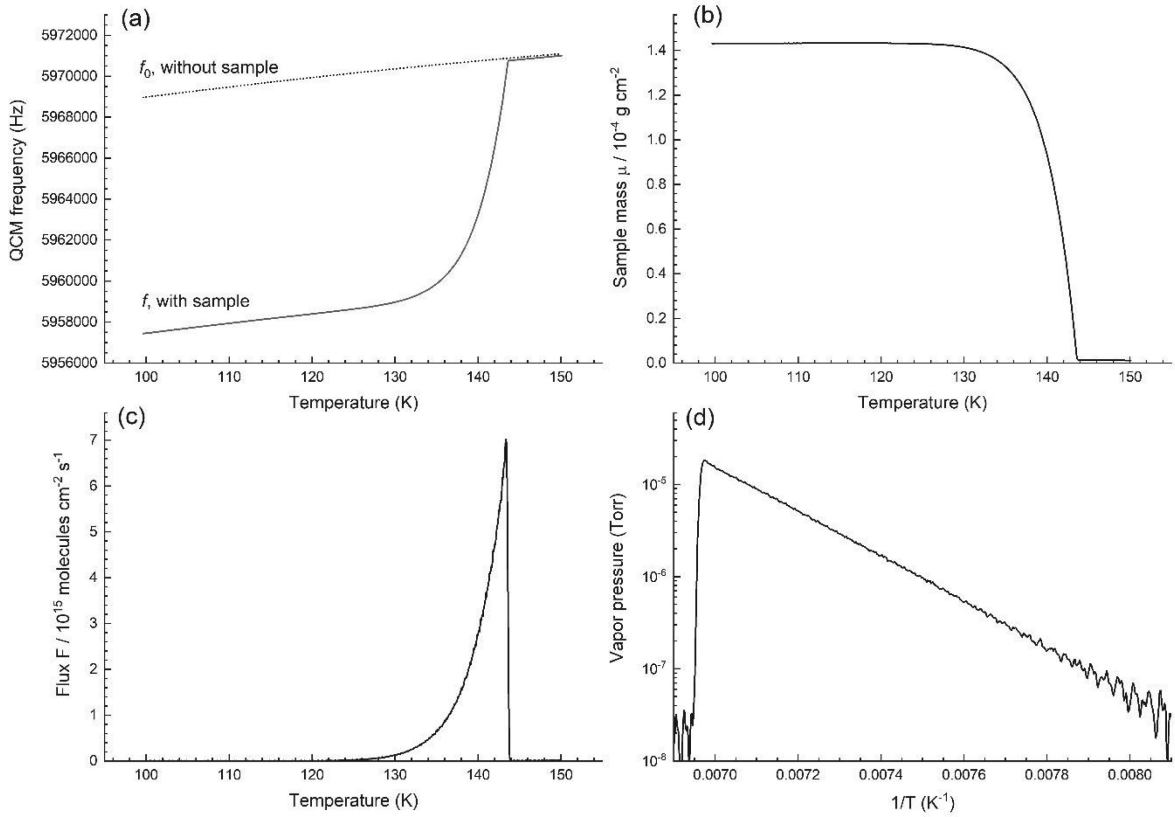

Figure 9. Results from warming crystalline propanal from 100 to 150 K. (a) QCM frequencies with (solid line) and without (dotted line) ice present, (b) the sample's mass per unit area on the microbalance, (c) the flux of subliming molecules, and (d) derived vapour pressure (on a logarithmic scale) vs 1/*T*.

Table 3. Enthalpy of sublimation and vapour pressures of crystalline propanal

$\Delta H_{\rm subl}$ (kJ mol^{-1})	Temperature (K)	Vapour pressure[a] (10^{-7} Torr)	Uncertainty[b] (10^{-7} Torr)
46.09 ± 0.03	120	0.0884	0.0030
	125	0.573	0.019
	130	3.21	0.10
	135	15.9	0.5
	140	70.1	2.2

[a]Vapour pressures derived from fits to ln(*P*) vs. 1/*T* (see the text).
[b]Uncertainties are from the propagation of the uncertainties in the fitting parameters. Percent uncertainties are about 3 per cent.

for any part of propanal's IR spectrum. It also is possible to use our optical constants to compute spectra obtained by reflection from a surface, assuming that the underlying substrate's *n* and *k* are known. In this way, optical constants are superior to band strengths alone as they can be used for a greater variety of applications.

The number of solid-phase aldehydes for which band strengths have been measured appears to be limited to our earlier work on acetaldehyde (Hudson & Ferrante 2020) and propynal (Hudson & Gerakines 2019). Tables in those papers show that for each compound the most-intense IR spectral feature of the amorphous ice is the carbonyl (C=O) stretch near 1700 cm^{-1}. Band strengths (*A*') of 2.98 × 10^{-17} and 2.80 × 10^{-17} cm molecule^{-1} for acetaldehyde and propynal, respectively, are comparable, but slightly higher, than for propanal (2.32 × 10^{-17} cm molecule^{-1}). However, the absorption coefficient (α') of propanal is about half that of the same quantity for the other two aldehydes.

4.3 Vapour pressures and enthalpy of sublimation

A lack of published data makes it is difficult to evaluate our measurements of solid propanal's sublimation energy and vapour pressures. The NIST data on this compound's liquid phase (https://webbook.nist.gov/chemistry/) give enthalpies of fusion and vapourization of about 9 and 31 kJ mol^{-1}, respectively, so that a rough approximation to a room temperature enthalpy of sublimation is ∼40 kJ mol^{-1}. Since a rise in sublimation energy might be expected with decreasing temperature, this value can be taken as a lower bound for $\Delta H_{\rm subl}$ for solid propanal near 145 K. We simply note that our $\Delta H_{\rm subl} \approx 46$ kJ mol^{-1} is above this value.

Evaluating our vapour pressure results is even more difficult. Fray & Schmitt (2009) reviewed solid-phase vapour–pressure data for 53 molecular species, but none on propanal or its next smaller (acetaldehyde) or larger (butanal) congener. Clearly, more measurements of solid-phase vapour pressures on a wider variety of compounds would enable better comparisons of the type needed here. At present all we can say is that the per cent uncertainties for the vapour pressures in our Table 3 are about 3 per cent.

4.4 APPLICATIONS

Applications of our data are similar to those described in our recent papers (e.g. Hudson & Ferrante 2020). Our α' and *A*' values will be useful in laboratory investigations of interstellar ice analogues, such as in measurements of initial abundances of propanal-containing ices or in estimating propanal reaction yields in photolytic, radiolytic, and other studies. Propanal composition

in ice mixtures, such as H_2O + propanal, can be determined accurately using our results for independent calibrations of each ice component without having to make assumptions about the composition of an ice compared to the composition of a gas mixture. Also, having accurate mid-IR intensities makes scaling to the intensities for the far- and near-IR regions more accurate. Solid propanal's two strong IR peaks in the 1700–1600 cm^{-1} region are unusual for aldehydes and other simple carbonyl-containing compounds, and can be used to help verify propanal's presence in an ice. Finally, we hope that our work will spur new calculations (e.g. DFT, *ab initio* methods) of IR intensities and comparisons to our experimental results. A reliable, accurate way to calculate IR band strengths of organic solids would be of considerable value, but to date the results have not been promising (e.g. Hudson & Mullikin 2019).

5 SUMMARY AND CONCLUSIONS

The knowledge of the chemical and physical properties of identified and candidate extraterrestrial molecules is essential for both laboratory investigations and theoretical modelling. The present study is one contribution to the on-going effort to make accurate measurements of such properties. In the present case, amorphous and crystalline propanal ices were prepared under vacuum by vapour-phase deposition, and both a density and a refractive index were measured for each form of the resulting solid. These quantities were used to determine two measures of spectral intensity for propanal ices, with the aid of newly recorded mid-IR transmission spectra. Optical constants were calculated for both the amorphous and crystalline ices. Vapour pressures for the crystalline ice were measured over a range of temperatures, from which an enthalpy of sublimation was obtained for propanal. Some applications of our new data are described.

ACKNOWLEDGEMENTS

We acknowledge the support of NASA's Planetary Science Division Internal Scientist Funding Program through the Fundamental Laboratory Research (FLaRe) work package at the NASA Goddard Space Flight Center. We also acknowledge the financial support of the NASA Astrobiology Institute through funding awarded to the Goddard Center for Astrobiology under proposal 13–13NAI7–0032. YYY thanks the NASA Postdoctoral Program for her fellowship.

REFERENCES

Abplanalp M. J., Gozem S., Krylov A. I., Shingledecker C. N., Herbst E., Kaiser R. I., 2016, PNAS, 113, 7727
Abdulgalil A. G. M. et al., 2013, Phil. Trans. A., 371, 20110586
Altwegg K. et al., 2017, MNRAS, 469, S130
de Marcellus P., Meinert C., Myrgorodska I., Nahon L., Buhse T., d'Hendecourt L. L. S., Meierhenrich U. J., 2015, PNAS, 112, 965
Dostert K.-H., O'Brien C. P., Mirabella F., Ivars-Barceló F., Schauermann S., 2016, Phys. Chem. Chem. Phys., 18, 13960
Frankiss S. G., Kynaston W., 1972, Spectrochim. Acta, 28A, 2149
Fray N., Schmitt B., 2009, Planet. Space Sci., 57, 2053
Goesmann F. et al., 2015, Science, 349
Guirgis G. A., Drew B. R., Gounev T. K., Durig J. R., 1998. Spectrochim. Acta, 54A, 123
Heavens O. S., 2011, Optical Properties of Thin Solid Films. 2nd edition, Dover, New York, NY p. 114. (Original printing: 1955, Butterworths Scientific Publ, London)
Hollis J. M., Jewell P. R., Lovas F. J., Remijan A., Møllendal H., 2004, ApJ, 610, L21
Hudgins D. M., Sandford S. A., Allamandola L. J., Tielens A. G. G. M., 1993, ApJS, 86, 713
Hudson R. L., Ferrante R. F., 2020, MNRAS, 492, 283
Hudson R. L., Ferrante R. F., Moore M. H., 2014, Icarus, 228, 276
Hudson R. L., Gerakines P. A., 2019, MNRAS, 482, 4009
Hudson R. L., Loeffler M. J., Yocum K. M., 2017a, ApJ, 835, 225
Hudson R. L., Loeffler M. J., Gerakines P. A., 2017b, J. Chem. Phys., 146, 0243304
Hudson R. L., Loeffler M. J., Ferrante R. F., Gerakines P. A., Coleman F. M., 2020, ApJ, 891, 1
Hudson R. L., Moore M. H., 2018, ApJ, 857, 1
Hudson R. L., Mullikin E. F., 2019, Spectrochim. Acta, 207A, 216
Jonusas M., Guillemin J.-C., Krim L., 2017, MNRAS, 468, 4592
Jungclaus G. A., Yuen G. U., Moore C. B., Lawless J. G., 1976, Meteoritics, 11, 231
Kaiser R. I., Maity S., Jones B. M., 2014, Phys. Chem. Chem. Phys., 16, 3399
Khanna R. K., Allen J. E., Masterson C. M., Zhao G., 1990, J. Phys. Chem., 94, 440
Krim L., Jonusas M., Guillemin J.-C., Yáñez M., Lamsabhi A. M., 2018, Phys. Chem. Chem. Phys., 20, 19971
Lu C., Lewis O., 1972, J. Appl. Phys., 43, 4385
Luna R., Millan C., Domingo M., Santonja C., Satorre M., 2012, Vacuum, 86, 1969
Lykke J. M. et al., 2017, A&A, 597, A53
McGuire B. A., 2018, ApJS, 239, 17
Moore M. H., Ferrante R. F., Moore W. J., Hudson R. L., 2010, ApJS, 191, 96
Murphy D. M., Koop T., 2005, Q. J. R. Meteorol. Soc., 131, 1539
Qasim D. et al., 2019, A&A, 627, A1
Sbrana G., Schettino V., 1970, J. Molec. Spec., 33, 100
Schuhmann M. et al., 2019, ACS Earth and Space Chem., 3, 1854
Smith T. E., Bonner R. F., 1951, Ind. Eng. Chem., 43, 1169
Tempelmeyer K. E., Mills D. W., 1968, J. Appl. Phys., 39, 2968

SUPPORTING INFORMATION

Supplementary data are available at *MNRAS* online.

Figure S1
Figure S2
Figure S3
Figure S4
Figure S5
Figure S6
Figure S7
Figure S8
Figure S9

Please note: Oxford University Press is not responsible for the content or functionality of any supporting materials supplied by the authors. Any queries (other than missing material) should be directed to the corresponding author for the article.

This paper has been typeset from a Microsoft Word file prepared by the author.